J. Phys. B: At. Mol. Opt. Phys. **21** (1988) 3929-3939. Printed in the UK

Multiple ionisation of rare gases by high-energy uranium ions†

H Berg‡, R Dörner‡, C Kelbch‡, S Kelbch‡, J Ullrich‡, S Hagmann§, P Richard§, H Schmidt-Böcking§, A S Schlachter‖, M Prior‖, H J Crawford‖, J M Engelage‖, I Flores‖, D H Loyd¶, J Pedersen+ and R E Olson#

‡ Institut für Kernphysik, Universität Frankfurt, D6000, Frankfurt, Federal Republic of Germany
§ Kansas State University, Manhattan, Kansas 66506, USA
‖ Lawrence Berkeley Laboratory, Berkeley, California 94720, USA
¶ Angelo State University, San Angelo, Texas 76909, USA
+ University of Aarhus, DK 8000 Aarhus, Denmark
# University of Missouri-Rolla, Rolla, Missouri 65401, USA

Received 13 May 1988, in final form 18 July 1988

Abstract. Multiple ionisation cross sections $\sigma(q)$ for the production of recoil ions in charge state q by 120 MeV u^{-1} U^{90+} impact have been measured for Ne, Ar and Kr targets using a recoil-ion-projectile-electron triple-coincidence technique. The data are compared with previously measured cross sections for U-ion impact in the projectile energy (E_P) range from 1.4 to 420 MeV u^{-1}. For low recoil-ion charge states $\sigma(q)$ decreases over the whole E_P range somewhat more slowly than $1/E_P$, whereas for higher recoil-ion charge states $\sigma(q)$ reaches a maximum at about 10-15 MeV u^{-1}. The data are nicely described by parameter-free n-body Classical Trajectory Monte Carlo (nCTMC) calculations. The calculations indicate the importance of accounting for the Auger events in the description of the multiple ionisation process. Because of the smooth E_P dependence of $\sigma(q)$ towards high E_P, the development of a recoil-ion source using a primary U-ion beam in a storage ring for the production of high charge state recoil-ions appears to be feasible.

1. Introduction

Multiple ionisation of target atoms by fast heavy-ion impact has attracted much interest in recent years. The development of new time-of-flight techniques by different groups (Cocke 1979, Groh *et al* 1981, Schlachter *et al* 1981, Hvelplund *et al* 1980, Damsgaard *et al* 1982, Kelbch *et al* 1985, Müller *et al* 1986) made measurements of differential cross sections for multiple ionisation possible. Theory (Olson 1987, Horbatsch 1986, Horbatsch and Dreizler 1986) also has achieved a breakthrough in describing the many-particle interactions in such encounters. Nevertheless, many aspects of the multiparticle interaction in encounters associated with large perturbation still remain unsolved: can the electrons be treated as independent particles, leading to binomial statistics with respect to the degree of multiple ionisation, or have electron-electron correlation effects a measurable influence on the $\sigma(q)$, where q is the final charge state

† Supported by: Bundesministerium für Forschung und Technologie (BMFT) under grant 060F/73 (741336476), Gesellschaft für Schwerionenforschung (GSI), NATO under grant RG85/0501 and Department of Energy (DOE).

0953-4075/88/233929+11$02.50

of the target recoil ion? Another problem is the interaction potential: is it similar to a Thomas–Fermi interaction, or do polarisation and deformation of the target electron cloud influence the collision dynamics of both the electrons and the heavy nuclei? All these effects determine the total multiple ionisation cross section $\sigma(q)$ and are very difficult to treat in a many-particle collision theory. By necessity, theoretical approaches describing the many-electron Coulomb interaction are simplified by several approximations. The theoretical approach of Horbatsch (1986) and Horbatsch and Dreizler (1986) uses an independent-electron model, i.e. no interactions between the electrons are considered. This method provides a numerical solution to the Vlasov equation for the three-body system, i.e. projectile, nucleus and electron. An initial phase space distribution is chosen to reproduce the static properties of the neutral target. Another method (Olson 1987) provides a classical solution to a model, which includes all the target electrons distributed within a microcanonical distribution, but also no electron–electron interaction. This classical model leads to interesting predictions of ionisation phenomena for high projectile charge states in fast collisions: due to the strong two-centre nuclear Coulomb force interaction the electron emission can be very anisotropic in comparison with ionisation by protons.

One goal of our systematic investigation of multiple ionisation processes is to obtain $\sigma(q)$ for U-ion impact over a wide projectile energy range (E_P). In particular, the dependence of $\sigma(q)$ on the charge state at different E_P is a measure of n-body effects. Besides this interest in the understanding of the fundamental mechanisms of multiple ionisation, the application of multiple ionisation as an efficient tool for the production of highly charged very slow (<10 eV) recoil ions by fast ions in a heavy-ion storage ring is of considerable importance for atomic physics. U-ion beams of lower energy might have higher ionisation power, particularly for the outer electrons. However, fast beams are needed in a storage ring, as beam loss due to charge exchange decreases strongly for higher E_P and has to be sufficiently small to ensure long ion storage times. Therefore, the multiple ionisation of noble gases for very high energy (120 MeV u^{-1}) U-ion impact was investigated in the present experiment. As will be discussed below, non-perfect beam focusing and vacuum conditions in the beam line of the Bevalac accelerator and background ionisation in walls, etc, made the detection of recoil ions in high charge states, produced in a gas target with densities below a few ng cm^{-2}, extremely difficult. A triple coincidence between recoil ions, projectile and electrons was essential to suppress, at least partially, the large ionisation yield of the background radiation.

2. Experiment

The measurement of recoil-ion production for Ne, Ar and Kr targets by 120 MeV u^{-1} U^{90+} was performed at the Bevalac accelerator at the Lawrence Berkeley Laboratory. The charge-state-selected U^{90+} beam was focused in the gas-target region to a beam spot of about 5–6 mm (FWHM). The U-ion beam passed a windowless thin gas target (5×10^{-5} to 4×10^{-4} Torr) and produced the recoil ions and electrons (see figure 1). The projectiles were detected about 3 m downstream of the target by a fast scintillation detector. Recoil ions were extracted and accelerated perpendicular to the direction of the U-ion beam in an electrostatic field (about 100 V cm^{-1}) over a length of 17 cm, then drifted in a quasi-field-free region, and could be deflected magnetically onto a two-dimensional position-sensitive channel-plate detector to separate low and

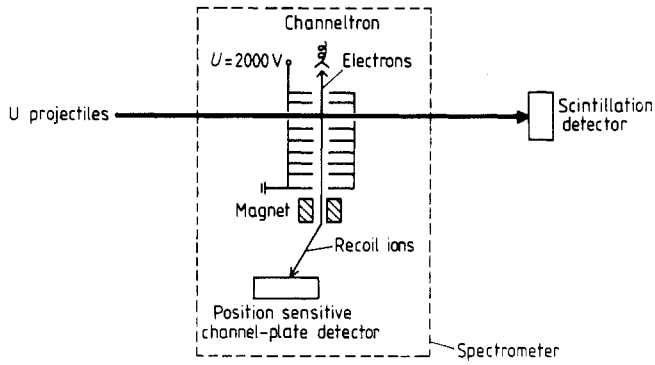

Figure 1. Experimental set-up.

high charge state recoil ions. Electrons emitted in the collision were accelerated in the opposite direction in the same field and were detected by a channeltron detector. The voltages on several slits between the extraction window and the channeltron could be varied independently to increase the electron-detection efficiency. The recoil-ion charge state was determined by a time-of-flight measurement (TOF), since the flight time t_R from the centre of the gas target to the detector is proportional to $1/\sqrt{q}$. The spectrometer was designed to use a large-diameter U beam ($\simeq$10 mm $\varnothing$). The gas-target region had an opening >20 mm, to allow transmission of the projectiles without direct impact on the apparatus. The dimensions of the recoil-ion extraction and drift region were designed to obtain optimum time focusing. The absolute time resolution τ was better than 4 ns and the relative resolution $\tau/t_R \simeq 10^{-3}$. Such time resolution with a large-diameter beam was necessary to suppress random background events. To obtain an even better suppression of the background, a triple coincidence with the electrons from the ionisation event was implemented. The electronic set-up is shown in figure 2. The events were stored on tape in list mode using the VME system (McParland and Bronson 1987).

A very large background was observed, predominantly associated with recoil-ion charge states $q=1$ and $q=2$. To reduce the triple-coincidence efficiency for these low

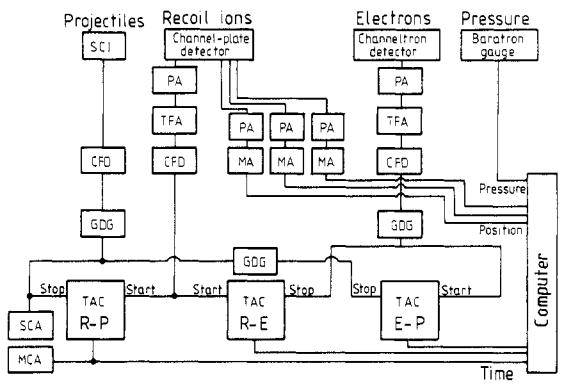

Figure 2. Schematic diagram of electronic arrangement. SCI: scintillator; GDG: gate and delay generator; PA: preamplifier; TAC: time-to-amplitude converter; MA: main amplifier; SCA: scaler; TFA: timing filter amplifier; MCA: multichannel analyser; CFD: constant fraction discriminator.

recoil-ion charge states, the efficiency to detect one electron was set to about three per cent. For a recoil ion in charge state q, q electrons are emitted to the continuum; the detection probability $P_e(q)$ is proportional to $1-(1-P_e(q=1))^q$. Thus for $q=10+$, a triple-coincidence efficiency of about 30% (see figure 3) could be obtained.

Figure 4 shows a recoil-ion–projectile coincidence spectrum for 120 MeV u^{-1} U^{90+} impact on Ar in comparison with a spectrum for 15.5 MeV u^{-1} U on Ar measured with a well collimated beam at the GSI Unilac (Kelbch *et al* 1985). The relative contribution of random coincidences for the 120 MeV u^{-1} U-ion impact is orders of magnitude higher than at the lower energies. Triple-coincidence data are shown in figure 5 (recoil-ion–projectile coincidence against recoil-ion–electron coincidence). The diagonal (III) represents the real triple-coincident events, where, for each recoil ion, the projectile and electrons released in the same event were detected. Regions I and

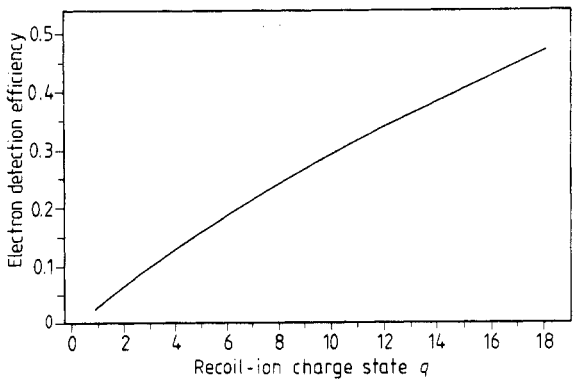

Figure 3. Calculated electron-detection efficiency as a function of the recoil-ion charge state q.

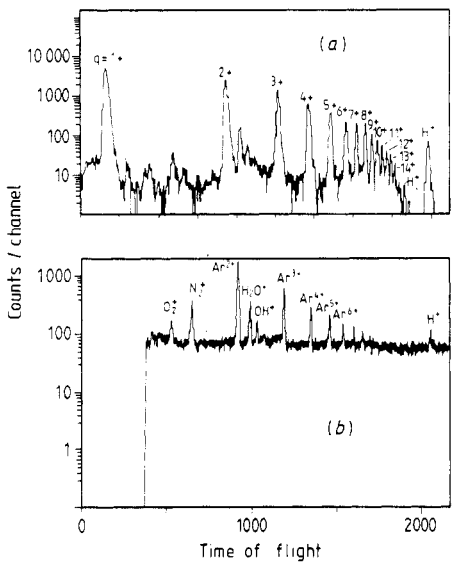

Figure 4. Comparison of recoil-ion–projectile time-of-flight spectra for (*a*) 15.5 MeV u^{-1} U^{75+} and (*b*) 120 MeV u^{-1} U^{90+} on Ar collisions.

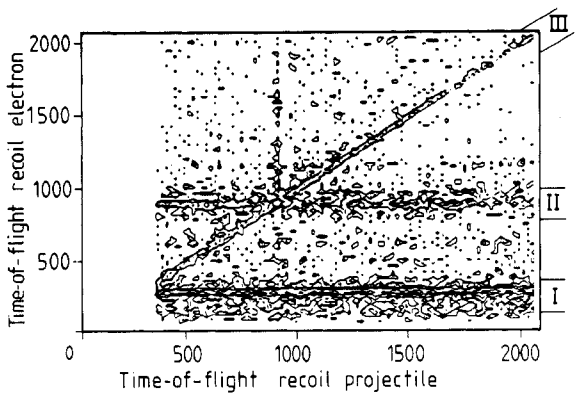

Figure 5. Two-dimensional contour plot of recoil-ion–projectile against recoil-ion–electron time-of-flight spectra for 120 MeV u^{-1} U^{90+} on Ar. The regions I, II and III are explained in the text.

II show the recoil-ion–electron coincidence for $q = 1+$ and 2+, for which the corresponding true projectile has not been detected (random events in the projectile detection). These recoil-ion–electron coincidences are produced by the very large x-ray and fast electron background flux, which ionises target-gas atoms in the whole target region, whereas 'real' recoil ions are merely produced in the track of the projectiles. The width of the time peaks of $q = 1+$ and 2+ recoil ions in the recoil-ion–electron TOF spectrum is much larger than in the recoil-ion projectile coincidence, indicating that these recoil ions are produced over the whole extraction length of the spectrometer. Figure 6 shows the dependence of the background yield on the target-gas pressure, from which we can deduce how these background x-rays and electrons are created. The linear dependence clearly indicates that these events are indeed produced by single collisons of x-rays and electrons with target atoms, rather than by double collision processes in the target gas. For a double collision (first step: x-ray and electrons are produced by the U ions in the gas; second step: $q = 1, 2$ ionisation of gas atoms by these x-rays and electrons) the yield would be proportional to the square of the pressure. Because of the long beam transport lines (>40 m) and a beam line pressure greater than 10^{-5} Torr, a small fraction (0.1–1%) of the projectile beam underwent charge exchange and gave rise to a wider halo of the beam due to different trajectories in the dipole and quadrupole magnets. Depending on the focusing conditions this fraction could be strongly reduced,

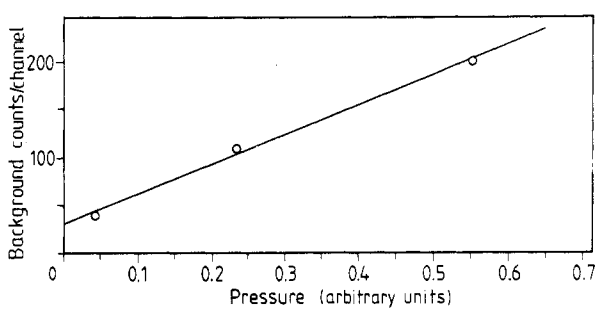

Figure 6. Gas-target pressure dependence of the 'background' yield in the recoil-ion $q = 1+$, 2+ charge states obtained in the recoil-ion–projectile coincidence.

but was always present even under the best beam conditions. If only 5–10 U ions per beam spill (every 6 s) hit the wall in the vicinity of the apparatus, millions of high-energy x-rays and electrons are produced, which ionise and produce a large number of low-charge-state recoil ions in the thin gas target.

The background can be strongly reduced by setting a diagonal window (III) in figure 5. Integration of the relevant recoil-ion charge-state peaks and correction with the electron detection efficiency yields the number of true events per charge state $N(q)$. To obtain absolute cross sections $\sigma(q)$ the total number of projectiles N_P was measured. The target gas pressure p was measured with a Baratron capacitive manometer. The recoil-ion detection efficiency, $\varepsilon\Delta\Omega_{Rec}/4\pi$ (ε efficiency of the channel-plate detector), multiplied by the effective gas-target thickness Δx monitored with a Baratron gauge, was measured independently at the 2.5 MV accelerator at the University of Frankfurt, using known charge-exchange cross sections for 2 MeV u^{-1} Ne^{2+} on Ne (Ullrich *et al* 1986). This normalisation was necessary, because the pressure profile in the target region was not exactly known due to the windowless gas-target system. The $\sigma(q)$ are calculated using equation (1):

$$\sigma(q) = N(q)4\pi/(N_P\Delta x p\varepsilon\Delta\Omega_{Rec}). \tag{1}$$

Figure 7 shows the recoil-ion distribution on the two-dimensional channel-plate detector indicating that the recoil-ion detector itself (40 mm diameter) and the recoil-ion extraction system yielded a nice recoil-ion beam spot and thus a controlled detection efficiency.

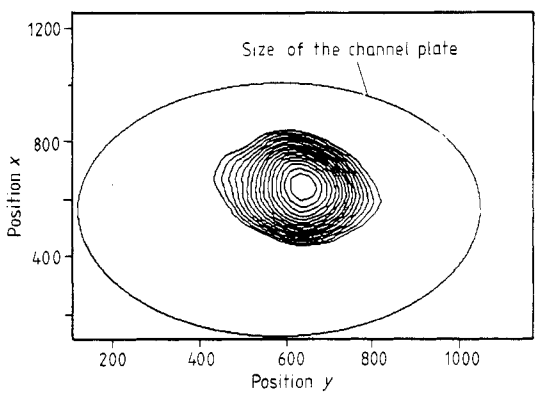

Figure 7. Two-dimensional position distribution of recoil ions on the recoil-ion channel plate detector. The z scale is logarithmic.

3. Data and discussion

Figure 8 presents the cross sections for recoil-ion production in Kr, Ar and Ne targets for 120 MeV u^{-1} U^{90+} impact. The error bars show only the statistical errors; the error in the absolute normalisation is estimated to be about 30%. The data were obtained at a pressure of $2\text{–}3\times10^{-4}$ Torr. For higher pressure (4.5×10^{-4} Torr) a 50% reduction of the highest charge-state rate was observed, indicating charge capture of the slow, highly charged recoil ions in the extraction region. Therefore, even the lower pressure data may somewhat (30–50%) underestimate the 'true' cross sections for high $q > 10$.

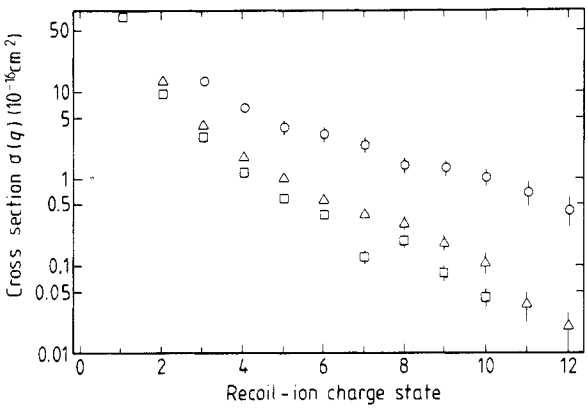

Figure 8. Measured total cross sections $\sigma(q)$ for 120 MeV u^{-1} U^{90+} on Ne (□), Ar (△) and Kr (○).

Figure 9 presents all available Ar ionisation data measured for U-ion impact from 1.4 to 420 MeV u^{-1} as a function of the projectile energy (Kelbch *et al* 1985, 1986, Müller *et al* 1986). Note that the normalisation of the data from Kelbch *et al* (1985), Richard *et al* (1985) and Ullrich *et al* (1984, 1987) has been twice remeasured with improved techniques, because the pressure meter (Baratron gauge) used in the first measurement (Kelbch *et al* 1985) had to be recalibrated. The single capture channel in the previous experiment also included small-angle and slit-scattering contributions due to a non-perfect projectile charge-state separation. The two new independent measurements with a 27 cm long gas cell yielded for the single electron capture cross section $\sigma(n = 55, n' = 54, 5.9\ \text{MeV u}^{-1}) = 7.96$ and 8.8×10^{-17} cm^2. Therefore, all $\sigma(q)$ in Kelbch *et al* (1985), Richard *et al* (1985) and Ullrich *et al* (1984, 1987) have to be divided by the factor 3.9. Furthermore, figure 3 in Kelbch *et al* (1985) and Richard

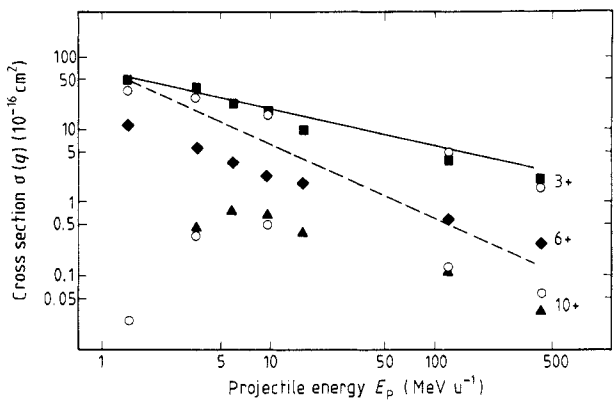

Figure 9. Projectile energy (E_p) dependence of the multiple ionisation cross sections $\sigma(q)$ for Ar (the full symbols represent the measured data for $q = 3+, 6+, 10+$). The U^{n+} charge states were $n = 44$ at 1.4 MeV u^{-1}, $n = 50$ at 3.9 MeV u^{-1}, $n = 55$ at 5.9 MeV u^{-1}, $n = 65$ at 9.4 MeV u^{-1}, $n = 75$ at 15.5 MeV u^{-1}, $n = 90$ at 120 MeV u^{-1} and $n = 91$ at 420 MeV u^{-1}. The full line shows the relative $1/\sqrt{E_p}$ and the broken line the $1/E_p$ dependence normalised to the experimental value $\sigma(q = 3, 1.4\ \text{MeV u}^{-1})$. The open circles represent *n*CTMC calculations for $q = 3+$ and $q = 10+$.

et al (1985) show the wrong scales (factor of 10 too small). The U charge states were $n = 50$ at 3.6 MeV u^{-1}, $n = 55$ at 5.9 MeV u^{-1}, $n = 65$ at 9.4 MeV u^{-1}, and $n = 75$ at 15.5 MeV u^{-1}.

The circles in figure 9 represent *n*CTMC calculations for $q = 3$ and $q = 10$. All calculated values shown were determined via the *n*CTMC method (Olson 1987), where the Ar K-, L- and M-shell electrons are explicitly included in the calculations. Auger effects are taken into account by calculating the total electronic energy of the residual Ar ion after the collision and assuming that the relaxation to the ground-state configuration occurs with 100% branching by multiple Auger decay. The Auger process is significant and is found to increase the final charge state of the recoil ions by more than one charge state.

All $\alpha(q)$ for $q < 8$ decrease smoothly with a slope between $1/v_P$ and $1/E_P$ for increasing E_P. Figure 9 also shows the relative $1/E_P$ and $1/v_P$ dependencies (broken and full lines). This behaviour is not expected from first-order perturbation theory since for lower q the energy dependence is predicted to be approximately proportional to $(1/E_P)^q$ for small perturbation (Inokuti 1971). For $q > 10$ the cross sections $\sigma(q)$ peak at $E_P \geq 10$ MeV u^{-1}. The maximum of the $\sigma(q)$ shifts towards higher E_P with increasing q. Therefore we expect that the $\sigma(q = 17, 18)$ cross sections for Ar continue to increase for $E_P > 15.5$ MeV/u and may reach a maximum at $E_P \simeq 20$–40 MeV u^{-1}.

Figure 10 presents a comparison of *n*CTMC calculations by Olson with the measured 120 MeV u^{-1} data for U-ion impact on Ar. The full curve represents the calculation, which includes autoionisation processes occurring after the collision. The broken curve shows the theoretical $\sigma(q)$ before autoionisation. The comparison of both values indicates that a considerable fraction of low-energy electrons will be produced in these collisions by Auger cascades occurring after the collision. The number of Auger electrons can be deduced from the theory but not from figure 10 directly, since a shift in the absolute height of the cross section as well as in the charge-state scale is involved. It is apparent from figure 9 that multiple ionisation cross sections are large compared with the dimension of the Ar atom. Ionisation probabilities exceed the 10% level by far (Ullrich *et al* 1988) at all projectile energies and thus, perturbation techniques are inappropriate to describe the collision mechanisms. The energy dependence of the $\sigma(q)$ cross sections predicted by the *n*CTMC theory is in good agreement

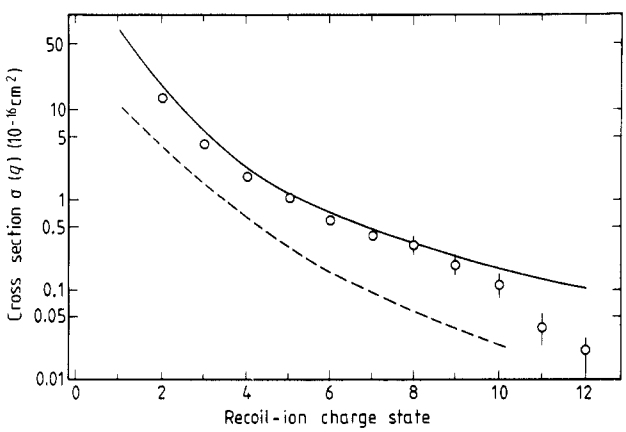

Figure 10. Comparison of measured $\sigma(q)$ with *n*CTMC calculations; ○, experiment; ——, autoionisation included; - - -, autoionisation not included.

with the experiment. Considering the complexity of this many-body process, the overall agreement is excellent, but still considerable information on scattering dynamics is to be gained from further studies of these collisions. In particular the extrapolation of calculated cross sections towards highest q and E_P is risky, because the contribution of autoionisation processes after the ionisation and excitation of a shell is not yet exactly known. Therefore it is necessary to measure the cross sections up to $q = Z_T$. The comparison with the calculated values is a crucial test for the correct implementation of Auger processes into theoretical models. Another problem is whether the classical electron picture is valid towards highest E_P, or whether wavepackets are needed to describe the electrons. To answer this question, it is essential to obtain data for highest q and E_P.

4. Prospects for a recoil-ion source at an U-ion storage ring

An U-ion storage ring beam provides an unique ionisation power to produce very cold highly charged ions (Ullrich *et al* 1984, 1987).

From the data and *n*CTMC calculations it is clear that outer-shell ionisation decreases towards high E_P, whereas inner-shell ionisation reaches a maximum at $E_P \simeq 2E_B M_P/m_E$, where E_B is the electron binding energy and M_P and m_E are the masses of projectile and electron respectively. The combination of outer- and inner-shell ionisation finally reduces $\sigma(q \to Z_T, E_P)$ for high-energy U-ion beams ($E_P >$ 100 MeV u^{-1}). Nevertheless, the data from figure 11, where the ratios $\sigma(q, E_P)/\sigma(q, E_P = 3.6$ MeV u$^{-1})$ normalised to the charge state Ar^{3+} are plotted, and the data from Kelbch *et al* (1985) and Richard *et al* (1985), where the absolute cross section up to $q = 18+$ for 15.5 MeV u^{-1} U^{75+} on Ar are shown, allow an extrapolation towards $\sigma(U^{90+} \to Ar,\ q = 17,\ E_P = 120$ MeV u$^{-1})$. The relative q dependence of $\sigma(q)$ is almost identical for 3.6, 120 and 420 MeV u^{-1}. Since for the inner shell we expect even higher ionisation cross sections at 120 than at 3.6 MeV u^{-1}, the ratio in figure 11 for higher charge states may be larger than 1 and may even approach, for $E_P \simeq$ 50 MeV u^{-1}, those for 9.4 and 15.5 MeV u^{-1}. Thus we estimate by extrapolation that

$$\frac{\sigma(\mathrm{Ar}, q = 17+, E_P = 120\ \mathrm{MeV\,u^{-1}})}{\sigma(3+, 120\ \mathrm{MeV\,u^{-1}})} = \frac{\sigma(17+, 15.5\ \mathrm{MeV\,u^{-1}})}{\sigma(3+, 15.5\ \mathrm{MeV\,u^{-1}})}.$$

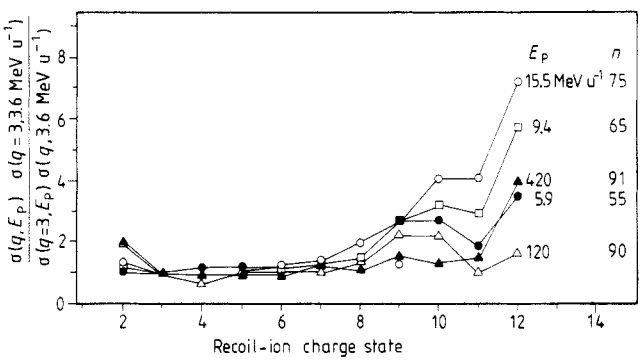

Figure 11. $[\sigma(q, E_P)/\sigma(q = 3, E_P)]/[\sigma(q, 3.6\ \mathrm{MeV\,u^{-1}})/\sigma(q = 3, 3.6\ \mathrm{MeV\,u^{-1}})]$ cross section ratio for U^{n+} on Ar as function of the recoil-ion charge state for various values of E_P (MeV u^{-1}).

For $\sigma(q=17+, E_P=120\ \text{MeV u}^{-1})$ we estimate a value of the order of $10^{-18}\ \text{cm}^2$.

For 5×10^{10} U ions stored in the storage ring, 2×10^6 cycles per second and a gas-target pressure of 3×10^{13} Ar atoms/cm^2, the number of Ar^{17+} ions can be estimated using the extrapolated cross section to be 3×10^{12} ions/s, or approximately 8 μA. This recoil-ion beam is known to have a very small energy spread since the recoil ions are produced with very small recoil-ion energy (Olson *et al* 1987). Since at this target pressure the 120 MeV u^{-1} U^{90+} beam will undergo several electron capture and loss processes per second, the U beam can be stored with acceptable storing periods (~minutes) only if the storage ring is capable of multiple charge transport. Since capture and loss are in equilibrium at $n=90$ the storage time can be enhanced strongly.

The recoil-ion yield can be improved by the construction of a solenoidal ion trap, where successive ionising collisions become possible. Pre-ionisation of the target considerably enhances the high-charge-state cross sections under storage ring conditions. The enhancement is energy dependent and is found (Olson 1987) to amount to only a factor of 1.3 at 9.4 MeV u^{-1}. However, it rises to $\sim10^3$ at 120 MeV u^{-1} and $\sim10^5$ at 420 MeV u^{-1}. The reason for this dependence is the rapidly decreasing probability with increasing energy for removing M-shell electrons. Using trapped ions as target, e.g. in an ECR trap, pre-ionisation of the target will greatly increase the hydrogenic and fully stripped Ar^{17+} and Ar^{18+} yields at storage ring energies.

In a solenoidal ECR trap, a two-stage device (figure 12) could be additionally used to efficiently remove the outer electrons of the target atom. The first ECR stage would produce low-charge-state ions, which are injected into the second stage, where they are further ionised by the RF and the U beam. As the ions are drifting in a solenoid (length ~1 m, trapping time several hundred ms), the efficiency for the production of very high charge states increases due to two factors. Firstly, the outer-shell electrons are already removed, which enhances the ionisation power of the U-ion beam and, secondly, the long trapping time in the solenoid increases the probability of multiple interactions with the U beam. For an ion trap device the charge exchange of the primary beam is reduced and multiple charge transport may not be necessary. On the basis of measured $\sigma(q)$, we believe that it is possible to reach a yield of Ar^{17+} in the order of several tens of μA. This indicates that such a combination could also provide an excellent source for the production of very highly charged Kr and Xe recoil ions.

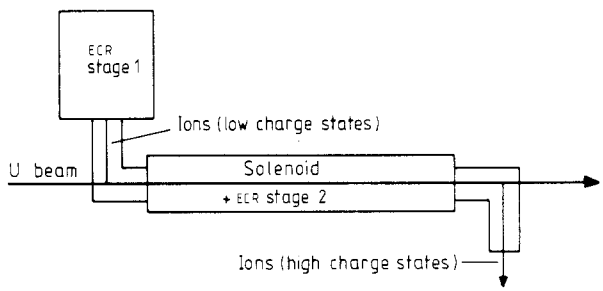

Figure 12. Scheme of a possible recoil ion source at a fast U-beam storage ring. Low ($q=1+, 2+$) charged recoil-ions are produced in the first stage of a two-stage ECR ion source and injected in the second stage. In the strong solenoidal field the recoil ions are trapped for several 100 ms. In this second stage the primary beam can further ionise the trapped recoil ions by successive collisions.

Acknowledgments

We thank Ch McParland and M Bronson for constructing and helping us with the VME system, and G Krebs, F Lothrop and the BEVALAC team for providing an excellent U-beam and helping us set up the beam line. Important parts of the apparatus were transported from Frankfurt to San Francisco through the generosity of Lufthansa. Support for our work was provided by the Director, Office of Energy Research, Office for Basic Energy Sciences, Chemical Sciences Division, US Department of Energy, contract No DE-AC03-76SF00098 (MHP, HS-B, RD, JP), Kansas State University (SH, PR, HS-B), Office of Fusion Energy—US Department of Energy (REO) and the NATO Science Fellowship Program (JP). Additional support was provided by the Friedrich Ebert Stiftung (RD) and NATO research grant No 0501/85 (HB, CK, HS-B).

References

Cocke C L 1979 *Phys. Rev.* A **20** 749
Damsgaard D, Haugen H K, Hvelplund P and Knudsen H 1982 *Phys. Rev.* A **27** 172
Groh W, Müller A, Achenbach C, Schlachter A S and Salzborn E 1981 *Phys. Lett.* A **85** 77
Horbatsch M 1986 *Z. Phys.* D **1** 337
Horbatsch M and Dreizler R M 1986 *Z. Phys.* D **2** 183
Hvelplund P, Haugen H K and Knudsen H 1980 *Phys. Rev.* A **22** 1930
Inokuti M 1971 *Rev. Mod. Phys.* **43** 279
Kelbch S, Ullrich J, Mann R, Richard P and Schmidt-Böcking H 1985 *J. Phys. B: At. Mol. Phys.* **18** 323
Kelbch S *et al* 1986 *J. Phys. B: At. Mol. Phys.* **19** L47
McParland C and Bronson M 1987 Private communication
Müller A, Schuch B, Groh W, Salzborn E, Beyer H F, Mokler P H and Olson R E 1986 *Phys. Rev.* A **33** 3010
Olson R E 1987 Private communication
Olson R E, Ullrich J and Schmidt-Böcking H 1987 *J. Phys. B: At. Mol. Phys.* **20** 1809
Richard P, Ullrich J, Kelbch S, Schmidt-Böcking H, Mann R and Cocke C L 1985 *Nucl. Instrum. Methods* **240** 532
Schlachter A S, Berkner K H, Graham W G, Pyle R V, Schneider P J, Stalder K R, Stearns J W and Tanis J A 1981 *Phys. Rev.* A **23** 2331
Ullrich J, Bethge K, Kelbch S, Schadt W, Schmidt-Böcking H and Stiebing K E 1986 *J. Phys. B: At. Mol. Phys.* **19** 437
Ullrich J, Cocke C L, Kelbch S, Mann R, Richard P and Schmidt-Böcking H 1984 *J. Phys. B: At. Mol. Phys.* **17** L785
Ullrich J, Horbatsch M, Dangendorf V, Kelbch S and Schmidt-Böcking H 1988 *J. Phys. B: At. Mol. Opt. Phys.* **21** 611
Ullrich J, Schmidt-Böcking H, Kelbch S, Berg H, Cocke C L, Hagmann S, Richard P, Schlachter A S and Mann R 1987 *Nucl. Instrum. Methods* B **23** 131